Highly Efficient Multichannel Spin-Polarization Detection

M. Kolbe,[1,*] P. Lushchyk,[1] B. Petereit,[1] H. J. Elmers,[1] G. Schönhense,[1] A. Oelsner,[2] C. Tusche,[3] and J. Kirschner[3]

[1]*Institut für Physik, Johannes Gutenberg-Universität Mainz, D-55128 Mainz, Germany*
[2]*Surface Concept GmbH, Am Sägewerk 23a, D-55124 Mainz, Germany*
[3]*Max-Planck-Institut für Mikrostrukturphysik, Weinberg 2, D-06120 Halle, Germany*

(Received 7 June 2011; published 8 November 2011)

Since the original work by Mott, the low efficiency of electron spin polarimeters, remaining orders of magnitude behind optical polarimeters, has prohibited many fundamental experiments. Here we report a solution to this problem using a novel concept of multichannel spin-polarization analysis that provides a stunning increase in efficiency by 4 orders of magnitude. This improvement was demonstrated in a setup using a hemispherical electron energy analyzer. An imaging setup proved the principal capability of resolving more than 10^5 data points in parallel.

DOI: 10.1103/PhysRevLett.107.207601 PACS numbers: 79.60.−i, 73.20.−r, 75.25.−j, 75.70.−i

Spin-polarization measurements of free electrons remain challenging since their first realization by Mott. As Heisenberg's uncertainty principle forbids the Stern-Gerlach experiment for free electrons, the determination of spin polarization relies on spin-orbit or exchange interaction. Electrons are scattered at solid state targets which reduces the efficiency by orders of magnitude compared to polarization analyzers for visible light.

Many emerging research fields are inaccessible with state-of-the-art spin detectors. Examples are single-shot experiments with extreme ultraviolet (XUV) laser pulses [1,2], nonrepetitive phenomena, fundamental spin interactions, e.g., in topological insulators [3], and spin-resolved hard-x-ray photoemission spectroscopy in the valence band region [4] to name but a few.

Here we show that our novel approach of two-dimensional multichannel spin detection overcomes this drawback with a uniquely high efficiency that is about 4 orders of magnitude enlarged in comparison to the performance of single-channel state-of-the-art electron spin detectors.

The relevant quantity for the statistical performance of a polarimeter is its figure of merit $\mathcal{F} = S^2 I/I_0$ with S being the asymmetry function (also termed Sherman function [5,6]) and I/I_0 the ratio of scattered versus incoming intensity. All present commercial spin-polarization detectors [7–9] are based on single-channel electron scattering and are characterized by a figure of merit of typically 10^{-4} since the early 1980s, when two of the authors employed Mott scattering in a gas-phase photoemission experiment [10] and introduced spin-polarized low-energy electron scattering (SPLEED) as an ultra high vacuum (UHV)-compatible method for spin polarimetry [11]. Typical widely used instruments are described in Ref. [12] (120 keV Mott detector), in Ref. [7,13] (SPLEED detector), and in Ref. [9] (mini-Mott detector). Only in few cases, higher efficiencies have been reported. One approach is the scattering from clean [14] oroxygen-passivated thin Fe [15,16] or Co [17] films, where 1–2 orders of magnitude can be gained. However, the elaborate preparation of high-quality Fe and Co films is a specialist's method and is so far only used by a few groups worldwide. As an alternative approach, spin-dependent electron transmission through ferromagnetic ultrathin films was proposed as a high-efficiency spin filter [18]. Such devices, though principally possible [19], pose the experimental problem to produce large, freestanding few nanometer thick films of Fe or Co.

In spin-integral electron spectroscopy the situation developed completely different. With the advent of multichannel detection, the efficiency of electron spectrometers increased strongly. Today, state-of-the-art electron energy analyzers feature highly efficient multichannel detection with more than 10^4 data points acquired simultaneously [20]. When comparing spin-resolved with spin-integral electron spectroscopy we thus face a difference in counting efficiency of 8 orders of magnitude. In practice, spin-resolved spectroscopy with sufficient count rates can often only be performed with strongly reduced energy and angular resolution.

The novel multichannel concept is based on the idea of preserving a two-dimensional electron distribution in the spin-polarized low-energy electron diffraction process. The analyzer crystal is mounted in specular geometry deflecting the electrons by 90°. The conservation of the electron momentum component parallel to the crystal surface, inherent to the (0,0) beam, guarantees a transfer of the two-dimensional lateral image information that is encoded in the scattering coordinates and angle.

Figure 1(a) shows a schematic view of the multichannel spin polarimeter setup attached to a hemispherical electron spectrometer. In its exit field the electron spectrometer separates the electrons by their energy in the dispersive direction. The nondispersive direction shows separated emission angles in the case of a modern spectrometer. We therefore name this the (reciprocal) angular direction.

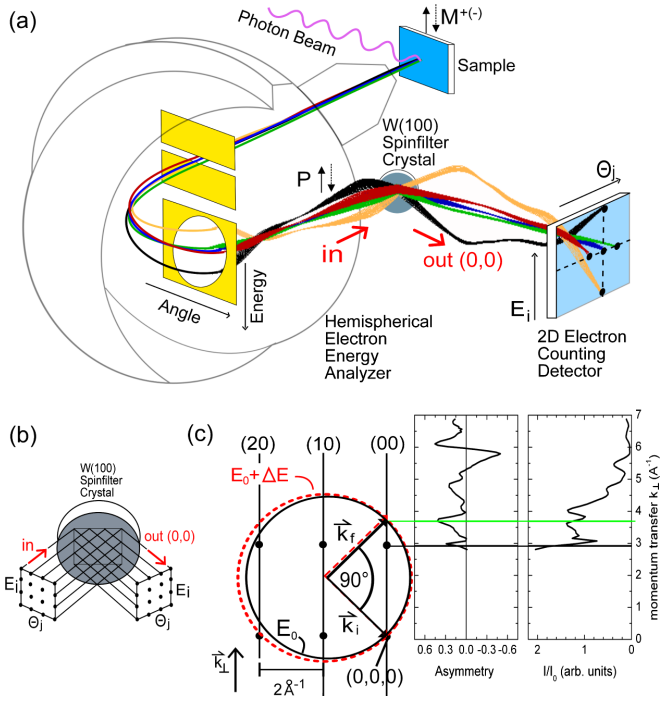

FIG. 1 (color online). (a) Schematic view of the multichannel spin polarimeter setup behind the exit field of a hemispherical analyzer comprising a narrow entrance slit and a wide exit field. Two of the trajectory bundles indicate electron paths separated along the energy axis E_i. The other bundles correspond to different emission angles separated along the Θ_j axis on the detector. (b) Geometry of the scattering process for simultaneous acquisition of 16 data points for the idealized case of a parallel beam and (c) corresponding momentum scheme (Ewald construction) in the kinematic approximation for specular reflection [(0,0) beam] for W(100) at 45° and 26 eV. A variation of E by 10% modifies the scattering condition (red).

The electron-optical simulation shows four bundles of trajectories calculated assuming perfect specular reflection from the surface of the W(100) spin filter crystal. In this geometry, the polarization component perpendicular to the scattering plane ($P^{\uparrow(\downarrow)}$) is analyzed via diffraction at about 26 eV kinetic energy. The spin filtered image is recorded by a delay line detector (DLD) [21] with a lateral resolution of about 50 μm and an active detection area of 40 mm diam. detecting single-electron events. The electron signal is intensified and the position is detected via runtime differences in a 2D meander. The whole assembly is contained in a magnetically shielded vacuum chamber.

The scattering process is sketched in Fig. 1(b) assuming a parallel beam. The specular (0,0) beam is used for spin filtering. Electrons penetrate ~4 monolayers into the crystal [22].

The momentum scheme is shown in Fig. 1(c), where we have indicated the interference structure along $\mathbf{k}_\perp$. Assuming an inner potential of 9 eV and accounting for a compression of the top layer spacing by 6% [23] yields a position of the first interference maximum at an impact energy of 16 eV. This means that the observed maximum at 25 eV results from multiple scattering. Because of spin-orbit coupling, the majority and minority electrons see different potentials, leading to different scattering amplitudes which govern the asymmetry function [5]. The figure reveals that a variation of E at fixed Θ (dotted lines) leads to a variation of the size of the Ewald sphere and hence, to a modification of the interference condition (intensity and asymmetry) as observed experimentally (see [24] for Supplemental Material). An analogous argument holds for a variation of the angle. The optimum working point for W(100) is at a scattering energy $E_0 = 26$ eV. There, we find a large reflectivity of 0.012 and an asymmetry of $S = 0.43$.

Figure 2 shows first experimental results of photoelectron spectra recorded from a clean Fe (100) sample excited by He I ($h\nu = 21.23$ eV) radiation. Figure 2(a) shows the lateral electron distribution pattern of photoelectrons emitted from the Fe(100) surface after being dispersed by the hemispherical energy analyzer and after scattering at the spin filter crystal. The energy-dispersive and angular

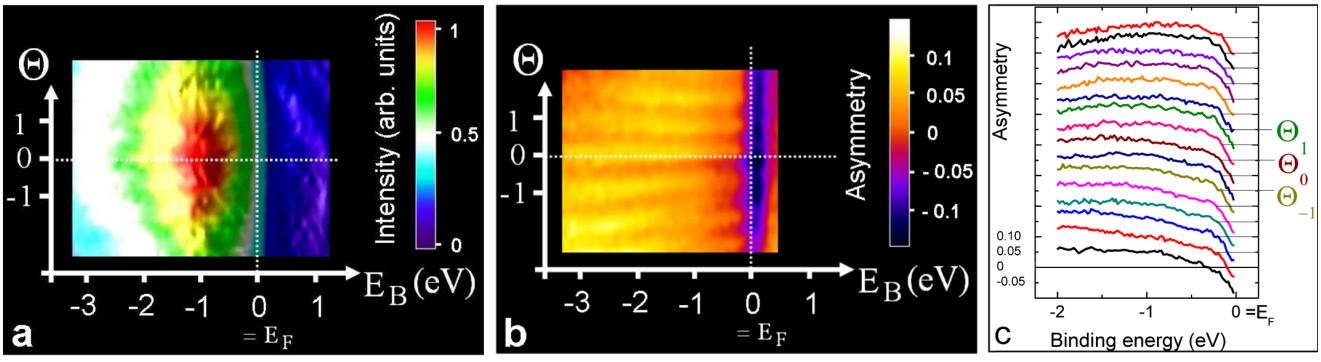

FIG. 2 (color online). (a) Two-dimensional electron intensity distribution (false color map) in the exit field of the electron spectrometer, imaged after reflection at the spin filter crystal. The spectrum corresponds to the 2D photoelectron distribution of an iron film near the Fermi edge ($h\nu = 21.23$ eV). (b) Corresponding asymmetry pattern calculated from two measurements with opposite magnetization directions of the iron film, cf. Eq. (1). The background was corrected linearly, the intensity variation in the dependence of Θ was not corrected. (c) Line scans of the asymmetry for different angular coordinates Θ_j.

resolving directions correspond to the axes E_i and Θ_j in Figs. 1(a) and 1(b), where indices i and j number the resolvable data points. The DLD registers each counting event with respect to its coordinate (E_i, Θ_j) yielding the accumulated count rate I_{ij}. The intensity cutoff on the right-hand side of Fig. 2(a) represents the Fermi edge (marked by the vertical dotted line) which could be displayed sharply, validating that no significant distortion of the ray bundles occurs during the diffraction process.

Figure 2(b) shows a typical asymmetry distribution pattern of Fe(100). The asymmetry is negative at the Fermi edge, turning to positive values at higher binding energies. The horizontal stripe pattern originates from a fine stripe mesh placed in the beam path of the analyzer optics. The stripe pattern shows the largest contrast in Fig. 2(b) as the shadow areas have zero asymmetry. We can resolve 16 bright and 16 dark (shadow) stripes with 2 image points each, leading to a minimum number of 64 resolvable angular intervals.

The width of the energy band across the exit field of the spectrometer is approximately 3 eV. For our room temperature measurements at 50 eV pass energy, we derive an energy resolution of about 180 meV, including the thermal broadening of 100 meV. This translates into a number of 17 resolvable energy points. This yields a total of 64 angular points $\times$ 17 energy points $=$ 1044 data points acquired simultaneously. In a different multichannel spin filter experiment using the same scattering arrangement in an emission electron microscope, approximately 3850 data points could be resolved [25].

The 2D spin-asymmetry pattern A_{ij} as shown in Fig. 2(b) is determined via pixel-by-pixel processing of two electron distribution patterns like Fig. 2(a), taken for opposite sample magnetizations. For each data point the spin polarization is determined as:

$$P_{ij} = A_{ij}\frac{1}{S_{ij}} = \frac{I_{ij}^{+} - I_{ij}^{-}}{I_{ij}^{+} + I_{ij}^{-}}\frac{1}{S_{ij}} \tag{1}$$

where $I_{ij}^{+(-)}$ denote the intensities in pixel (i, j) for sample magnetization directions $+$ $(-)$ and S_{ij} is the asymmetry function. For details on the energy dependent function S_{ij} see [24].

Figure 2(c) shows line profiles of the measured asymmetry vs kinetic energy extracted from Fig. 2(b) at different angles Θ_j. With a modern hemispherical analyzer, the Θ_j axis corresponds to different emission angles, which typically range from $-7°$ to $+7°$ [20]. For the given photon energy it is thus possible to investigate 30% of the Brillouin zone of the iron sample with one image [15 minutes acquisition time with the quality as in Fig. 2(a)].

In order to compare the new multichannel spin polarimeter to state-of-the-art single-channel spin detectors for electron spectroscopy, we define the "two-dimensional figure of merit" $(\mathcal{F}_{2D})$ as the product of the single-channel $\mathcal{F}_{\text{single}}$ averaged over the energy interval acquired simultaneously multiplied by the number of resolved data points N, i.e.,

$$\mathcal{F}_{2D} = N\langle\mathcal{F}_{\text{single}}\rangle = N\left\langle S_{ij}^2\frac{I_{ij}}{I_{ij,0}}\right\rangle. \tag{2}$$

For an energy interval of 3 eV we found a value of $\mathcal{F}_{2D} = 1044 \times 1.7 \times 10^{-3} \simeq 1.8$ with $\langle S_{ij}\rangle = 0.38$ and the averaged effective intensity response $\langle I_{ij}/I_{ij,0}\rangle = 1.2\%$. This value is the highest found so far for electron spin polarimeters. It means that the multichannel detector is 10^4 times more efficient than a single-channel detector with a $\mathcal{F}_{\text{single}}$ in the range of 10^{-4} at the same resolution. When selecting a smaller energy interval of only 1 eV, $\langle S_{ij}\rangle$ increases to 0.41 which corresponds to a $\mathcal{F}_{2D} = 2.1$ (see [24]).

A typical set of spin-resolved spectra for the Fe(100) surface is shown in Fig. 3. The partial intensities for majority and minority electrons at the angular coordinate Θ_0 were determined via

$$I_{i,0}^{\uparrow(\downarrow)} = (1 \pm P_{i,0})I_{\text{tot},i,0} \tag{3}$$

where $I_{\text{tot},i,0}$ is the spin-integrated count rate $(I_{i,0}^{+} + I_{i,0}^{-})$ at the energy $E_{i,0}$ and $P_{i,0}$ is the polarization as given in Eq. (1).

The Fe spectra in Fig. 3 are characterized by a highly positive spin polarization of the prominent emission feature at a binding energy of 0.7 eV and a steep drop of the spin polarization to large negative values when approaching the Fermi energy due to a surface state in the minority electron band. These spectra agree perfectly well with spin-resolved He I spectra from the literature [26] for thin Fe films. This proof-of-principle shows that the spin filter works properly.

The present study was performed using a hemispherical analyzer that is not optimized for multichannel operation. Using state-of-the-art spectrometers the performance can

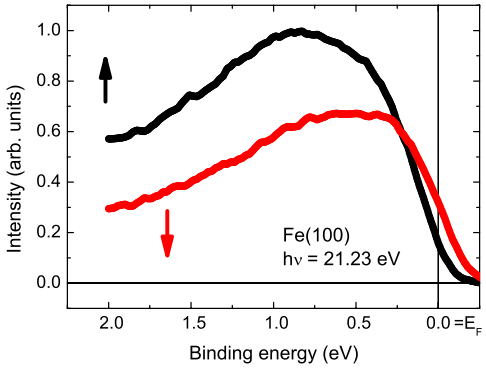

FIG. 3 (color online). Spin-resolved spectra ($h\nu = 21.23$ eV) near the Fermi edge of a clean Fe(100) surface. The up (down) arrow denotes majority (minority) partial spectra.

be improved considerably. The number of resolvable points is limited by the transfer width of the setup, the electron-optical aberrations, and by the mosaic spread of the tungsten single crystal. Because of the mosaic spread, an ideal parallel incident electron beam will be diffracted into a cone with an angle of 0.1°, using a typical value for a W(100) single crystal, translating to a spatial deviation of 0.16 mm in the image plane. This limits the number of resolvable image points to approximately 15 000, leading to a theoretical two-dimensional figure of merit of 19. Modern electron spectrometers provide 140 angular points and 200 energy points simultaneously [20]. Thus, for an optimized design we may expect a total gain ($\mathcal{F}$ and N) of more than 5 orders of magnitude compared to conventional spin detectors. W(100) with its optimum working point (26 eV scattering energy, $S = 0.43$, $I/I_0 = 1.2\%$) was chosen due to its ease of preparation. Other materials might offer higher $\mathcal{F}$s. For example, the problem of the mosaic spread could be avoided by epitaxial films on high-quality single crystal substrates.

As for all spin polarimeters it is advantageous to reverse the asymmetry. In the present work, the magnetization direction was reversed. Alternatively, the spin filter crystal–DLD assembly could be pivoted about the beam axis by $0° \mid 180°$ or $+90° \mid -90°$ to detect both transversal polarization components. Other spin-rotator assemblies were already successfully incorporated in spin-polarized low-energy electron microscopes [27].

For single-shot experiments that require a fully parallel image acquisition of a large electron flux arriving simultaneously at the detector, the DLD can be replaced by a multisegment detector or by an optical detector with CCD camera coupled to a fluorescent screen. In pulsed experiments, an additional condition can be set that eliminates all scattered electrons.

Besides the use for electron spectrometry the new multichannel approach can be used for momentum microscopy [28] and for spin-resolved imaging of Fermi surfaces.

In summary, we have developed a new type of multichannel spin polarimeter that shows an efficiency improved by about 4 orders of magnitude in comparison to state-of-the-art single-channel spin detectors. One order is gained by the high asymmetry function of $S = 43\%$ and the high reflectivity and 3 orders are gained by the multichannel approach. The figure of merit (1.7 reached, 19 expected for an optimized design) exceeds that of a ''perfect'' (Stern-Gerlach-type) single-channel spin filter ($\mathcal{F} = 1$). This gain in measuring efficiency paves the way to new experiments in various fields of current and future interest.

We thank O. Schaff (SPECS GmbH) for providing data of the exit parameters of the Phoibos analyzer and M. Jourdan for his help with the experiment. Financial support by Deutsche Forschungsgemeinschaft (SCHO 341/9-1, DFG-JST (FE633/6-1) and SFB/Transregio 49), and Stiftung Rheinland-Pfalz für Innovation (Project No. 886) is gratefully acknowledged. One of the authors (G. S.) would like to express his deep gratitude to J. Kessler for numerous enlightening discussions on the many aspects of spin-polarization detection.

*hahnmi@uni-mainz.de

[1] Y. Huismans, A. Rouze, A. Gijsbertsen, J. H. Jungmann, A. S. Smolkowska, P. S. W. M. Logman, F. Lpine, C. Cauchy, S. Zamith, T. Marchenko, J. M. Bakker, G. Berden, B. Redlich, A. F. G. van der Meer, H. G. Müller, W. Vermin, K. J. Schäfer, M. Spanner, M. Yu. Ivanov, O. Smirnova, D. Bauer, S. V. Popruzhenko, and M. J. J. Vrakking, Science **331**, 61 (2010).

[2] C. La-O-Vorakiat, M. Siemens, M. M. Murnane, H. C. Kapteyn, S. Mathias, M. Aeschlimann, P. Grychtol, R. Adam, C. M. Schneider, J. M. Shaw, H. Nembach, and T. J. Silva, Phys. Rev. Lett. **103**, 257402 (2009).

[3] Y. L. Chen, J. G. Analytis, J.-H. Chu, Z. K. Liu, S.-K. Mo, X. L. Qi, H. J. Zhang, D. H. Lu, X. Da, Z. Fang, S. C. Zhang, I. R. Fisher, Z. Hussain, and Z.-X. Shen, Science **325**, 178 (2009).

[4] Z. Boekelheide, A. X. Gray, C. Papp, B. Balke, D. A. Stewart, S. Ueda, K. Kobayashi, F. Hellman, and C. S. Fadley, Phys. Rev. Lett. **105**, 236404 (2010).

[5] J. Kessler, *Polarized Electrons* (Springer-Verlag, Berlin, 1985), 2nd ed..

[6] J. Kirschner, *Polarized Electrons at Surfaces*, Springer Tracts in Mod. Phys. (Springer-Verlag, Berlin, 1985), Vol. 106.

[7] D. Yu, C. Math, M. Meier, M. Escher, G. Rangelov, and M. Donath, Surf. Sci. **601**, 5803 (2007).

[8] G. Ghiringhelli, K. Larsson, and N. B. Brookes, Rev. Sci. Instrum. **70**, 4225 (1999).

[9] T. J. Gay, Adv. At. Mol. Opt. Phys. **57**, 157 (2009).

[10] G. Schönhense, Phys. Rev. Lett. **44**, 640 (1980).

[11] J. Kirschner and R. Feder, Phys. Rev. Lett. **42**, 1008 (1979).

[12] U. Heinzmann, J. Phys. B **11**, 399 (1978).

[13] J. Garbe, D. Venus, S. Suga, C. M. Schneider, and J. Kirschner, Surf. Sci. **178**, 342 (1986).

[14] F. U. Hillebrecht, R. M. Jungblut, L. Wiebusch, C. Roth, H. B. Rose, D. Knabben, C. Bethke, N. B. Weber, S. Manderla, U. Rosowski, and E. Kisker, Rev. Sci. Instrum. **73**, 1229 (2002).

[15] A. Winkelmann, D. Hartung, C.-T. Chiang, and J. Kirschner, Rev. Sci. Instrum. **79**, 083303 (2008).

[16] T. Okuda, Y. Takeichi, Y. Maeda, A. Harasawa, I. Matsuda, T. Kinoshita, and A. Kakizaki, Rev. Sci. Instrum. **79**, 123117 (2008).

[17] C. Jozwiak, J. Graf, G. Lebedev, N. Andresen, A. K. Schmid, A. V. Fedorov, F. El Gabaly, W. Wan, A. Lanzara, and Z. Hussain, Rev. Sci. Instrum. **81**, 053904 (2010).

[18] G. Schönhense and H. C. Siegmann, Ann. Phys. (Leipzig) **505**, 465 (1993).

[19] W. Weber, S. Riesen, and H. C. Siegmann, Science **291**, 1015 (2001).

[20] http://www.specs.de (supplemented by information from O. Schaff, SPECS GmbH).

[21] A. Oelsner, O. Schmidt, M. Schicketanz, M. Klais, G. Schönhense, V. Mergel, O. Jagutzki, and H. Schmidt-Böcking, Rev. Sci. Instrum. **72**, 3968 (2001).
[22] M. Seah and W. Dench, Surf. Interface Anal. **1**, 2 (1979).
[23] R. Yu, H. Krakauer, and D. Singh, Phys. Rev. B **45**, 8671 (1992).
[24] See Supplemental Material at http://link.aps.org/supplemental/10.1103/PhysRevLett.107.207601 for the energy dependence of S and I/I_0.
[25] C. Tusche, M. Ellguth, A. Ünal, C.-T. Chiang, A. Winkelmann, A. Krasyuk, M. Hahn, G. Schönhense, and J. Kirschner, Appl. Phys. Lett. **99**, 032505 (2011).
[26] M. Getzlaff, J. Bansmann, and G. Schönhense, Phys. Rev. Lett. **71**, 793 (1993).
[27] T. Duden and E. Bauer, Rev. Sci. Instrum. **66**, 2861 (1995).
[28] B. Krömker, M. Escher, D. Funnemann, D. Hartung, H. Engelhard, and J. Kirschner, Rev. Sci. Instrum. **79**, 053702 (2008).